Open Access Library Journal
2025, Volume 12, e14260
ISSN Online: 2333-9721
ISSN Print: 2333-9705

Remote Sensing of Dust Deposition on Solar Panels: Assessing the Impact of Climate Variables in Sub-Saharan Africa—A Case Study in Mali

Yaya Dembélé[1,2*], Abdoul Latif Bonkaney[3], Souleymane Sanogo[2], Navneet Kumar[4], Bernhard Tischbein[4], Saïdou Madougou[3]

[1]West African Science Service Centre on Climate Change and Adapted Land Use (WASCAL), Doctoral Research Program in Climate Change and Energy (DRP-CCE), University Abdou Moumouni (UAM), Niamey, Niger
[2]Laboratory of Optics, Spectroscopy and Atmospheric Sciences (LOSSA), University of Sciences, Techniques and Technologies of Bamako (USTTB), Bamako, Mali
[3]Department of Physics, Ecole Normale Supérieure, University Abdou Moumouni, Niamey, Niger
[4]Division of Ecology and Natural Resources Management, Center for Development Research (ZEF), University of Bonn, Bonn, Germany
Email: *yayadembeledjita725@gmail.com

How to cite this paper: Dembélé, Y., Bonkaney, A.L., Sanogo, S., Kumar, N., Tischbein, B. and Madougou, S. (2025) Remote Sensing of Dust Deposition on Solar Panels: Assessing the Impact of Climate Variables in Sub-Saharan Africa—A Case Study in Mali. *Open Access Library Journal*, **12**: e14260.
https://doi.org/10.4236/oalib.1114260

Received: September 9, 2025
Accepted: November 4, 2025
Published: November 7, 2025

Copyright © 2025 by author(s) and Open Access Library Inc.
This work is licensed under the Creative Commons Attribution International License (CC BY 4.0).
http://creativecommons.org/licenses/by/4.0/
Open Access

Abstract

The study applied remote sensing techniques to detect dust deposits on photovoltaic solar panels in Kita, Mali, using the Google Earth Engine (GEE) platform. Sentinel-2 images (2021-2023) recorded on the GEE platform were used to derive sand indices, including the Ratio Normalized Difference Soil Index (RNDSI) and the Dry Bare Soil Index (DBSI), enabling monthly detection of dust accumulation patterns. Results indicate DBSI values ranging from 0.05 to 0.35 and RNDSI from 0.02 to 0.34. Seasonal trends were evident: June to September corresponded to the least dusty months, favoring optimal production, while December to May marked peak dust accumulation, highlighting critical periods for intensified cleaning and maintenance. The remote sensing analysis further provided the spatial distribution of deposited dust, allowing operators to target specific areas for prioritized cleaning interventions. By identifying both seasonal and spatial variations, this approach supports more efficient resource allocation and performance optimization of large-scale PV systems. Our findings demonstrate that freely available satellite data, combined with semi-automated GEE processing, is a cost-effective and near-real-time alternative to labor-intensive manual monitoring. This method can guide companies in planning a regular maintenance schedule improving long-term system efficiency,

and sustaining reliable solar energy production in dust prone environments.

Subject Areas

Energy and Environment

Keywords

Remote Sensing Techniques, Google Earth Engine, Monitoring, Dust Deposition, Solar Photovoltaic, Sand Indices

1. Introduction

The global transition to renewable energy highlights the urgent need to address environmental and operational challenges affecting photovoltaic (PV) efficiency. A key concern is soiling, where dust and dirt deposition can reduce PV performance by up to 50% in arid and semi-arid regions such as the Middle East and Sub-Saharan Africa [1] [2]. Mitigation requires location specific strategies, including tailored cleaning regimes [3] [4], and the adoption of advanced technologies. Remote sensing, image based systems, and AI-driven approaches offer promising tools for dust detection and automated monitoring [5]-[7]. Environmental studies confirm that wind dynamics, dust composition, and deposition processes significantly influence PV degradation [8] [9], while automated systems help quantify impacts and optimize maintenance [10] [11]. Other challenges such as Potential Induced Degradation (PID) further reinforce the need for integrated approaches [12].

In regions with severe dust exposure, case studies stress region specific interventions, such as post dust storm cleaning in Saudi Arabia [13] [14], and research on dust mineralogy (e.g., calcium carbonate) that exacerbates heating and efficiency losses [8] [15]. Proactive measures, particularly in arid areas with limited rainfall, are essential, including drone based imaging and AI-based cleaning optimization [16]-[18]. Long-term analyses reveal that unmaintained systems face substantial productivity losses [19], with dust reducing power output by 20% within 11 weeks in monocrystalline modules [20]. Collectively, these findings underscore the importance of continuous innovation and adaptive maintenance strategies to safeguard PV efficiency under diverse environmental conditions.

Despite these advancements, the application of remote sensing (RS) to PV performance monitoring in Sub-Saharan Africa remains underdeveloped. RS has been widely applied for tracking solar expansion [21], and for environmental monitoring, including erosion, desertification, and sand encroachment [22]-[24], as well as soil attribute management [25]. Yet, its integration into PV performance assessment remains limited [26], with most monitoring focused on utility-scale plants and little attention to smaller systems or microgrids [27]. This gap is significant given the growing deployment of solar power across the region.

In Mali, where scarce rainfall and water shortages complicate dust management, platforms such as Google Earth Engine (GEE) provide an opportunity to track dust deposition using soil and sand indices. This study applies GEE to monitor dust accumulation from 2021 to 2023, assessing seasonal variability and the influence of climate variables, including temperature, humidity, precipitation, and wind speed, on dust dynamics. Identifying high-risk periods and dust-prone hotspots enables the design of efficient cleaning schedules that balance panel performance with water conservation. By combining RS technology with climate analysis, this study proposes a practical framework for reducing dust related efficiency losses and enhancing the sustainability and reliability of solar power generation in arid regions.

2. Material and Methods

Study Area and Power Plant

The study area comprises a solar power plant, located in Kita, a town located in the southwestern region of Mali, 180 km from Bamako (**Figure 1**). It covers an area of 100 hectares (ha) at a latitude of 13.03˚N, and a longitude of −9.52˚W. The plant are on-grid systems which produce electricity and inject into the national electricity grid.

In Mali, Akuo Energy has commissioned the Kita solar power plant. The 50 MW infrastructure comprising 187,000 polycrystalline photovoltaic modules, was built 180 km west of the capital Bamako and has been in operation since March 2020. Its production supplies 120,000 Malian households. The generated electricity is sold to the Malian electricity company under 30-year power purchase agreement. At the Kita plant, PV modules are installed with a 15˚ tilt, oriented due south to optimize solar capture for the site's latitude and seasonal irradiance. Routine cleaning is conducted by the operator, but dust accumulation during the Harmattan and irregular rainfall patterns still lead to localized soiling hotspots across the array. Kita is characterized by a semi-arid climate with a distinct dry season (October to May) and a rainy season (June to September). During the dry season, strong winds from the Sahara Desert transport dust particles towards Kita, leading to significant dust deposition on surfaces, including solar panels. The region is a prime location for solar energy development, as it receives abundant sunlight year-round. However, the high dust deposition rates pose a significant challenge to the efficient operation of solar installations.

3. Data Used

3.1. Satellite Data (from 2021 to 2023)

The Sentinel 2 satellite data from 2021 to 2023 at monthly time steps were utilized to estimate the soiling indices of panels for a selected power plant using the Google Earth Engine (GEE), developed by Google Inc. GEE is an open, cloud-based geo-

spatial processing platform primarily designed for planetary-scale environmental data analysis.

Sentinel-2 (S2) is a wide-swath, high-resolution multispectral imaging mission that offers a global revisit frequency of every 5 days. The S2 Multispectral Instrument (MSI) captures data across 13 spectral bands: visible and near-infrared (NIR) at 10 meters, red edge and shortwave infrared (SWIR) at 20 meters, and atmospheric bands at 60 meters' spatial resolution. This data is suitable for assessing the condition and changes in vegetation, soil, and water cover.

The Sentinel 2 data bands (3, 4, 8, 12) were used to develop normalized difference sand index (NDSI) and ratio normalized difference soil index (RNDSI) with a spatial resolution of 10 meters and 20 meters. Band 3 (green band) and band 11 (short wave infra-red 1), were used to calculate the dry bare soil index (DBSI). The DBSI also involved using band 4 (red) and band 8 (near infra-red) to generate the normalized differential vegetation index (NDVI). The data acquisition and semi-automated processing of the images were completed on the GEE platform and the direct results of the images were extracted from the cloud-based platform. The detailed equations for deriving the soiling ratio indices are described below in the methodology section 4.2.

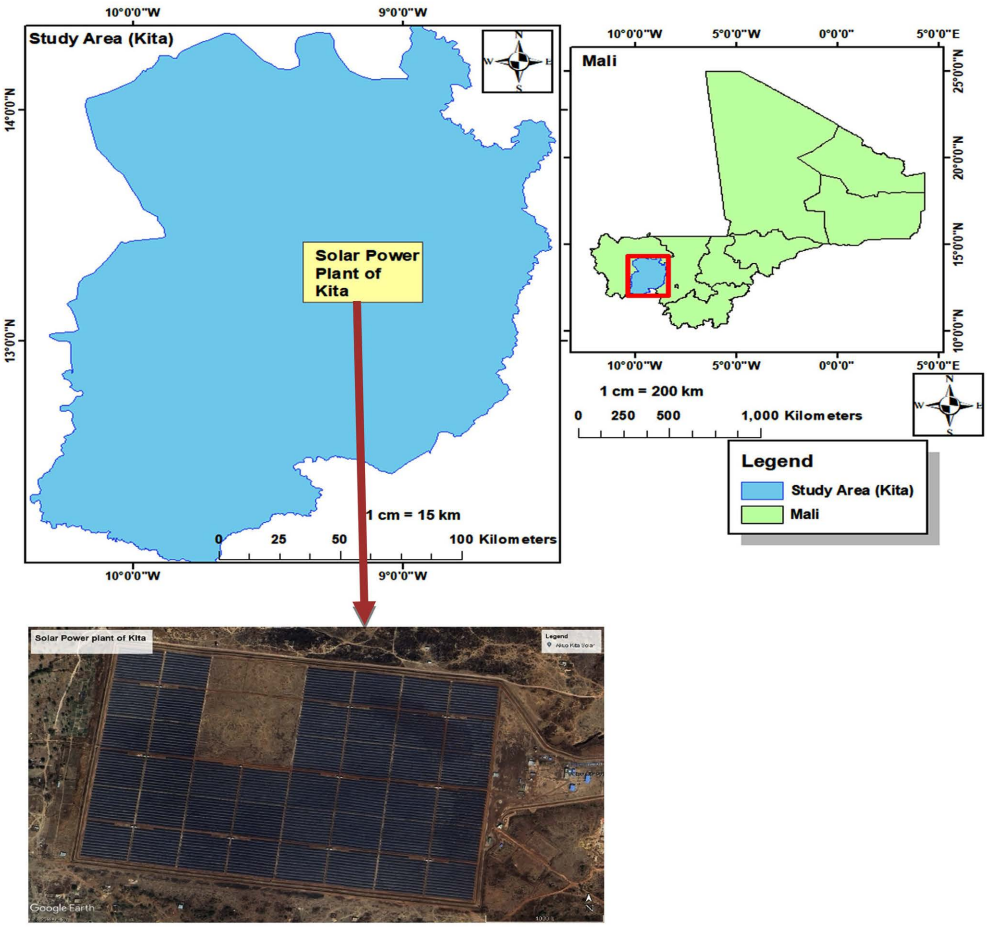

Figure 1. Location of the study area, the installed solar power plant.

3.2. Climate Variables

We have collected climate data on temperature, relative humidity, irradiance, wind speed, and precipitation, spanning from 1991 to 2022. The climate data were extracted from the Nasa Power database of daily measures at 0.5˚ × 0.625˚ grid resolution.

The climate variables are 1) temperature (˚C) Air temperature at a height of 2 meters above the surface. 2) Precipitation flux Total volume of liquid water (mm^3) precipitated over the period 00 h - 24 h local time per unit of area (mm^2), per day. 3) Wind speed ($m \cdot s^{-1}$) at a height of 10 meters above the surface over the period 00 h - 24 h local time. 4) Solar radiation flux ($Kwh/m^2/day$) Total amount of energy provided by solar radiation at the surface over the period 00 h - 24 h local time per unit area and time. 5) Relative humidity (%) Relative humidity at a height of 2 meters above the surface.

Dust data, Dust Surface Mass Concentration (DUSMASS) was obtained using NASA's Giovanni platform (EARTHDATA). The data, derived from MERRA-2 satellite reanalysis, covers the period from 1991 to 2022, with a spatial resolution of 0.5 × 0.625˚ and hourly temporal resolution.

3.3. Temporal Alignment

Climate statistics for the Kita site were analyzed over the 1991-2022 period to provide a robust baseline of temperature, irradiance, and wind speed conditions. By contrast, dust mapping using RNDSI/DBSI was limited to 2021-2023, reflecting the period of reliable Sentinel-2 availability and overlap with plant operation. This mismatch may reduce the strength of direct correlations between dust and climate variables; however, the approach remains valid, as dust dynamics during 2021-2023 can be interpreted within the context of the long-term climatological baseline.

4. Methodology

The methodology used in this paper is depicted as a flowchart in **Figure 2**. **T**he study used GEE to detect soiling on solar PV panels using Sentinel-2 satellite data, using two indices.

Furthermore, the climate variables were considered to explore the relationship with the dust deposition on the solar panels.

4.1. Exploratory Data Analysis (EDA)

First, exploratory data analysis is used to determine the distribution, seasonal trends, and interrelationships of the climate variables (irradiance, precipitation, relative humidity, temperature, and wind speed) with dust deposition. This entails detecting patterns or anomalies in the dataset that may affect dust deposition on photovoltaic (PV) panels.

Correlation analysis was applied, which quantifies relationships between variables using the Pearson Correlation Coefficient (PCC) or Spearman Correlation

Coefficient, depending on the data type. The Pearson correlation coefficient (PCC), often denoted as τ, is a measure of the linear relationship between two variables. It quantifies how closely the data points in a scatterplot align with a straight line. This measure is widely used in statistical analyses to determine the strength and direction of the association between variables [28].

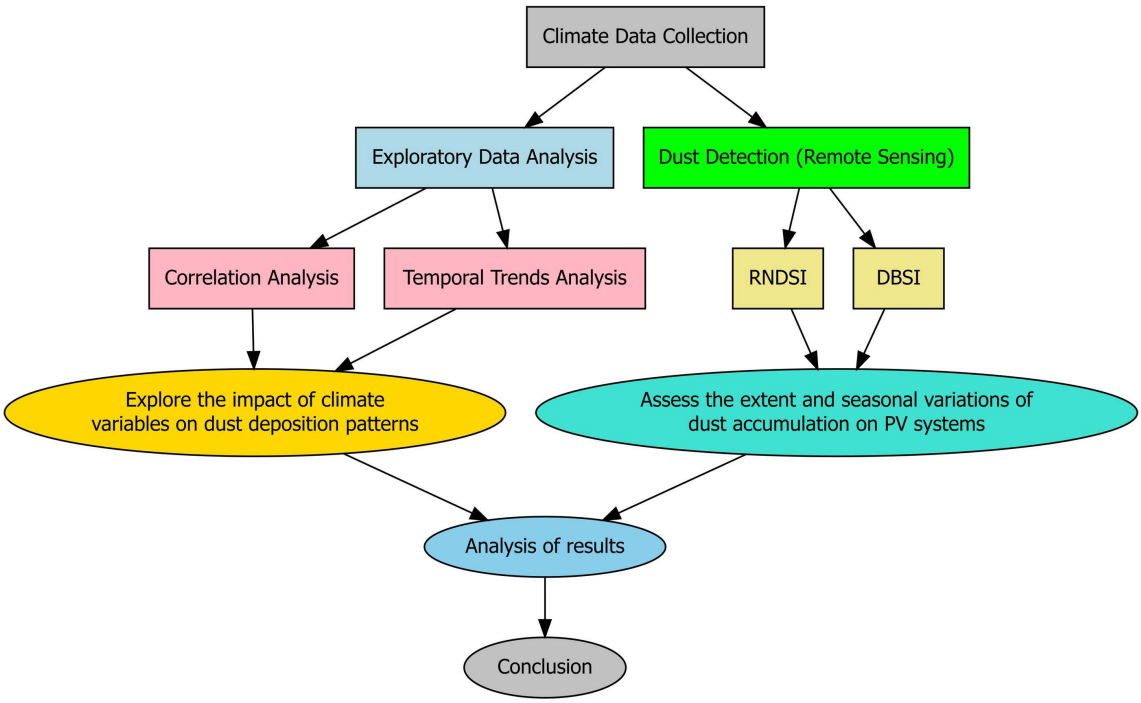

Figure 2. Flowchart of the study used to analyse relationships with climate parameters and detect soiling on PV solar panels.

To calculate the Pearson correlation coefficient, one must first understand its formula:

$$\tau = \frac{\sum (x_i - \overline{x})(y_i - \overline{y})}{\sqrt{\sum (x_i - \overline{x})^2 \sum (y_i - \overline{y})^2}} \tag{1}$$

here, x_i and y_i are the individual data points for variables X and Y, and $\overline{x}$ and $\overline{y}$ are the mean values of X and Y. The numerator of the formula represents the covariance between X and Y, while the denominator is the product of their standard deviations. This normalization ensures that τ lies between −1 and +1 [28].

The computation of τ involves the following steps. First, calculate the mean of X and Y using their respective data points. Then, subtract these means from each data point to center the data. Next, calculate the covariance by multiplying the deviations of X and Y, then summing these products. To compute the variances of X and Y, square the deviations of each variable and sum the results. Finally, divide the covariance by the product of the square roots of these variances (the standard deviations).

Once τ is computed, it can be interpreted as follows: $\tau = +1$ indicates a perfect positive linear relationship, where increases in X correspond to proportional increases in Y. Conversely, $\tau = -1$ signifies a perfect negative linear relationship, where increases in X correspond to proportional decreases in Y. An $\tau = 0$ implies no linear relationship between the variables.

The strength of the correlation can also be categorized. A correlation is considered strong when $0.7 \le |r| \le 1.0$, moderate when $0.3 \le |r| < 0.7$, and weak when $0.0 \le |r| < 0.3$. [28] This categorization provides insights into the degree of association and aids in interpreting the relationship between variables effectively.

Temporal Trends: Exploring seasonal patterns and climate anomalies to understand their impact on sand and dust deposition. These findings pave the way for future spatial and remote sensing analyses.

Results were visualized through graphs to highlight temporal and spatial patterns. Geographic Information System (GIS) tools were employed to overlay climatic variables map on the RNDSI and DBSI maps, derived by remote sensing in section 4.2, providing a clear representation of their relationships.

4.2. Methods of Detecting Dust Deposits on Panels Using Remote Sensing

4.2.1. Ratio Normalized Difference Soil Index (RNDSI)

The RNDSI characterizes the desert sand, which can help determine the level of fine sand deposition origin from the Sahara. Unlike vegetation, there are no spectral chain responses for soil due to its complex regional differences [29]. The two indices used are the Normalized Differential Soil Index (NDSI) and the Cap Transformation 1 (CT1) [30]. Here, RNDSI takes into account the image brightness effect derived from the cap transformation [29]. The first task is to calculate the ground index using a green band and two short-wave infrared bands from Sentinel-2 satellite data.

$$\mathrm{NDSI}_2 = \frac{\left(\mathrm{SWIR}_2 - \mathrm{Red}\right)}{\left(\mathrm{SWIR}_2 + \mathrm{Red}\right)} \tag{2}$$

The above result *i.e.*, NDSI_2 is further transformed to normalized NDSI_2 or NNDSI_2 (see Equation (3)). Then the NNDSI_2 is divided by a tasseled cap transformation brightness factor (NTCT). The mathematical expression of RNDSI is as follows:

$$\mathrm{NNDSI}_2 = \frac{\left(\mathrm{NDSI}_2 - \mathrm{NDSI}_{2\min}\right)}{\left(\mathrm{NDSI}_{2\max} + \mathrm{NDSI}_{2\min}\right)} \tag{3}$$

And

$$\mathrm{NTCT1} = \frac{\left(\mathrm{TC1} - \mathrm{TC1}_{\min}\right)}{\left(\mathrm{TC1}_{\max} - \mathrm{TC1}_{\min}\right)} \tag{4}$$

$$\mathrm{RNDSI} = \frac{\left(\mathrm{NNDSI}_2\right)}{\left(\mathrm{NTCT1}\right)} \tag{5}$$

The range of RNDSI values depends on the $TCT1_{min}$ and $TCT1_{max}$ values. In this case, the range of values selected for tasseled cap transformation brightness depends on the study area. Consequently, the final output, that is, the RNDSI has values that vary from 0.05 to 0.34. The higher the value of RNDSI , the higher the amount of soiling.

4.2.2. Dry Bare Sand Index (DBSI)

The Dry bare soil index (DBSI) is used to identify bare soil in arid and semi-arid regions, particularly in dry climate zones. A recent study [29] developed this index to map built-up and bare areas in dry climates using Landsat 8 data. In this study, the DBSI was applied to GEE values using Sentinel-2 data. Sentinel-2 images have a higher spatial resolution than Landsat images and are therefore more accurate in detecting sand deposit layers. The equation proposed for the nudity zone in a dry climate is the inverse of the modified normalized water difference index [29].

$$\mathrm{DBSI} = \frac{(\mathrm{SWIR1} - \mathrm{Green})}{(\mathrm{SWIR1} + \mathrm{Green})} - \mathrm{NDVI} \tag{6}$$

where,

$$\mathrm{NDVI} = \frac{(\mathrm{NIR} - \mathrm{Red})}{(\mathrm{NIR} + \mathrm{Red})} \tag{7}$$

A threshold value is used to differentiate between bare and non-naked soil areas in the city of Erbil, Iraq [29]. Based on a test with a sample of bare soil pixels, a DBSI value of 0.26 or more was defined as bare soil [29]. In this context, we will use the DBSI on the assumption that it can differentiate between dirty and clean pixels in our study area. In this study the DBSI value is between 0.05 and 0.35.

The RNDSI/DBSI threshold values (0.05 - 0.35) used in this study are partly informed by precedent in the literature. For example, [1] identified DBSI ≈ 0.26 as an effective boundary for differentiating soiled vs. cleaned PV module surfaces in a remote sensing study. The threshold range also aligns with observed soiling loss magnitudes in dry/desert or semi-arid conditions [31], where moderate soiling becomes performance limiting above similar index values. We further performed internal sensitivity tests on sample pixels from the Kita plant: thresholds below 0.05 failed to reliably separate clean from lightly soiled states, while thresholds above ~0.35 overstated soiling effects relative to observed directional losses.

Direct validation of RNDSI/DBSI outputs with ground-based data (e.g., inverter logs, on-site soiling ratios) was not possible due to restrictions imposed by the plant operator and managing agencies. This limitation is further discussed in the Discussion Section.

5. Results

5.1. Comprehensive Analysis of Dust Mass Surface Concentration (DUSMASS) in Relation to Climate Variables

The provided graphs collectively analyze the relationships between dust mass (kg/m^3) and five key environmental parameters: irradiance, precipitation, relative

humidity, temperature, and wind speed. Each parameter contributes to a nuanced understanding of Saharan dust dynamics and their interactions with atmospheric and climatic conditions.

5.1.1. Daily and Monthly Variations in Climatic Parameters and Dust Deposition

Dust strongly modulates solar irradiance by scattering and absorbing sunlight. As shown in **Figure 3(a)**, irradiance declines between October and January when dust levels are highest, particularly during storm events when dense layers restrict incoming radiation and induce localized cooling across the Sahara and adjacent regions. Seasonal variability is evident, with summer months recording higher irradiance due to fewer clouds and reduced dust compared to spring and winter.

Figure 3(b) shows that while temperature influences atmospheric dynamics, dust concentration in Kita is more directly controlled by wind strength, humidity, and rainfall. High dust levels coincide with the cooler, dry Harmattan season, while the rainy season suppresses dust despite lower temperatures.

Wind speed, highlighted in **Figure 3(c)**, is a key driver of dust activity. Moderate winds are most effective at mobilizing and sustaining airborne particles, while very strong winds disperse them over wider areas, reducing local concentrations. Peaks in wind speed from October to May coincide with high surface dust mass, underlining the importance of dry-season winds in sustaining dust transport.

Figure 3(d) demonstrates the cleansing role of precipitation. Rainfall during June-September sharply reduces dust through wet deposition, while the absence of rain in the dry season (October-May) allows concentrations to build and persist.

Relative humidity (**Figure 3(e)**) shows an inverse relationship with dust: higher humidity during the rainy season promotes particle aggregation and settling, while dry-season conditions (low humidity) favor dust suspension and uplift.

Together, these dynamics illustrate the combined influence of irradiance, wind, rainfall, and humidity in shaping dust seasonality and its implications for solar PV performance.

5.1.2. Combine Effects of Climate Variables on Dust Deposition

The interaction between climate variables highlights a coherent framework for Saharan dust dynamics. Dust uplift and transport are primarily controlled by wind speed, with moderate winds most effective when soils are dry and humidity is low. Soil moisture plays a critical role, as values above 3% - 4% substantially increase the threshold wind speed required for dust emission, making drier soils more vulnerable to wind-driven uplift [31]-[33].

Dust removal mechanisms operate mainly through precipitation and humidity, which reduce atmospheric dust via wet deposition and particle aggregation. Rainfall amount and intensity govern deposition efficiency, while humidity influences interparticle forces, with low humidity favoring the release of fine particles [34]-[36].

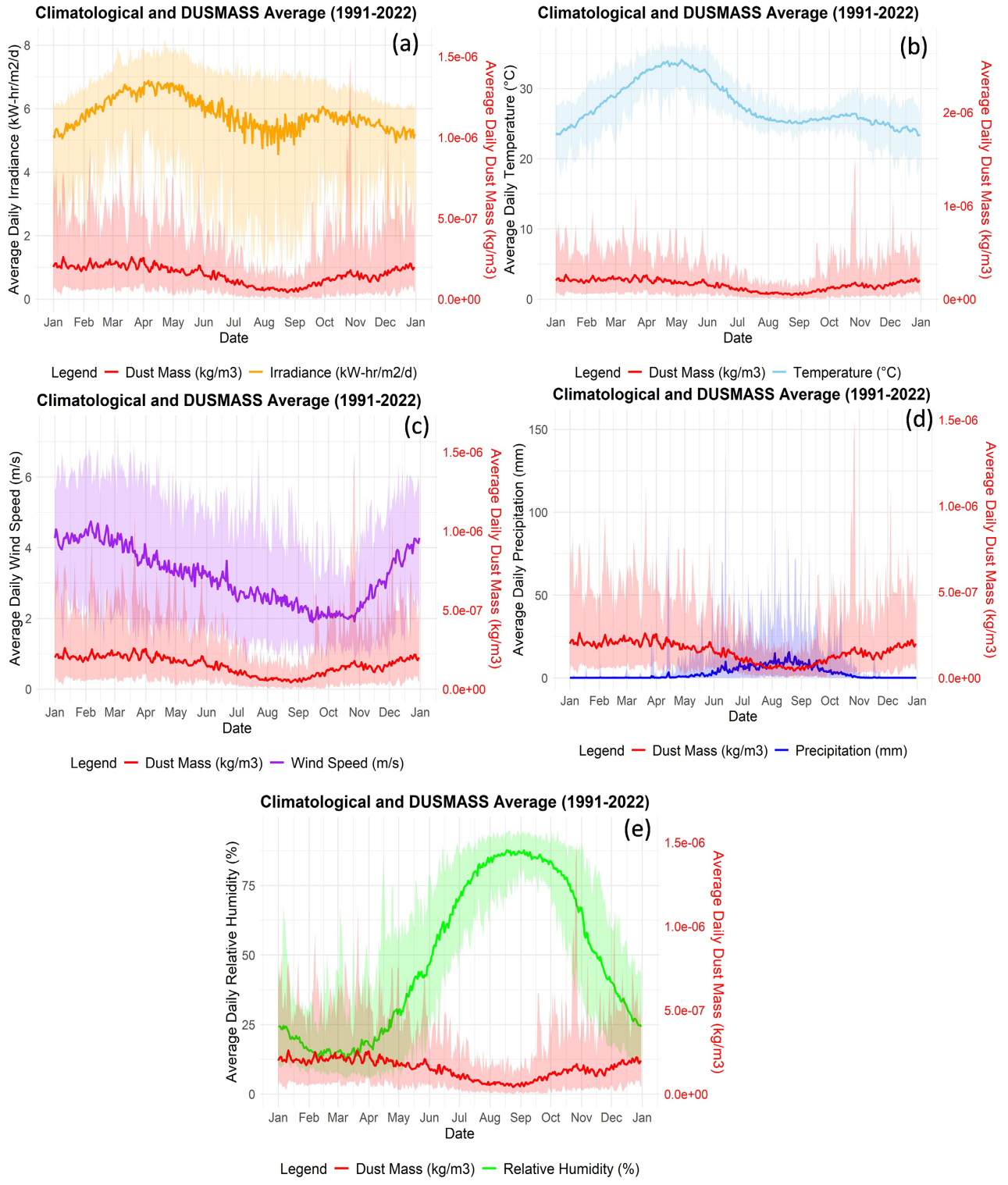

Figure 3. Daily and monthly variations in climatic parameters and dust deposition (DUSMASS) representing an average time period from 1991 to 2022: (a) DUSMASS and irradiance; (b) DUSMASS and Temperature; (c) DUSMASS and Wind Speed; (d) DUSMASS and Precipitation; (e) DUSMASS and Relative Humidity.

Climatic feedbacks arise because dust scatters and absorbs solar radiation, low-

ering surface irradiance and altering the radiative energy balance. This dual effect cools the surface but warms the atmosphere, modifying vertical and horizontal temperature gradients [37] [38]. Observations show surface cooling of up to 4 K during daytime dust events, with nighttime warming as heat is retained, while mid-tropospheric absorption promotes temperature inversions that suppress convection and influence rainfall and circulation patterns [39] [40].

Finally, seasonal patterns reveal peak dust concentrations during dry, windy months (December-May), when Harmattan winds dominate, and sharp declines during the wet season (June-September), when rainfall and high humidity enhance deposition. This seasonality is consistent with shifts of the Intertropical Convergence Zone (ITCZ), which modulates the alternation between dry northeasterly and moist monsoonal flows [41]-[43].

5.2. Analysis of the Pearson's Correlation Map of Climate Variables

The Pearson correlation matrix (**Figure 4**) highlights how environmental factors interact to shape dust dynamics in the study area. Dust concentrations show a strong positive correlation with wind speed ($r = 0.81$), confirming wind as the main driver of dust uplift and transport, particularly in dry seasons. In contrast, dust correlates negatively with precipitation ($r = -0.85$) and relative humidity ($r = -0.92$), reflecting the suppressing effects of rainfall and moisture on airborne dust. Moderate positive links are observed between dust and irradiance ($r = 0.47$) and dust and temperature ($r = 0.37$), suggesting that clear, warm, and dry conditions favor dust activity. Other parameter interactions further reinforce environmental coherence, such as the strong negative relationship between wind and humidity ($r = -0.91$), the positive association between precipitation and humidity ($r = 0.81$), and the alignment of irradiance with temperature ($r = 0.87$). Together, these correlations underscore the combined influence of climate variables on seasonal dust variability and PV performance.

5.3. Dust Maps Using Ratio Normalized Difference Soil Index (from 2021 to 2023)

The RNDSI maps for 2021, 2022, and 2023 (**Figures 5(a)-(c)**) provide a comprehensive view of the spatial and temporal variability of dust deposition on PV panels. RNDSI values are classified into three categories: low (2021-2022: −0.02 to 0.21; 2023: −0.05 to 0.21, green), moderate (0.21 - 0.22, yellow), and high (2021: 0.22 - 0.35; 2022: 0.22 - 0.37; 2023: 0.22 - 0.36, red).

In 2021 (**Figure 5(a)**), peak deposition occurred in December-March and again in October-November, periods when reduced rainfall and strong winds favored soiling, while June-September showed predominantly low values due to rainfall and vegetation growth. The 2022 (**Figure 5(b)**) maps revealed similar seasonal dynamics, with highest dust loads in December-February (February being the peak), persistence into March-May, and subsequent reductions in June-September. A resurgence of high values was observed in October, before conditions im-

proved slightly in November. In 2023 (Figure 5(c)), elevated RNDSI values again dominated the dry season (December-March), while June-September displayed widespread low values reflecting rainfall-driven cleaning. October-November showed a moderate increase linked to the seasonal transition from wet to dry conditions.

Across all three years, the results consistently identify December-March as the most critical period for dust accumulation and PV cleaning, with October-November acting as transitional months where monitoring remains necessary. Conversely, June-September emerges as the least demanding period for maintenance, as rainfall naturally suppresses dust and stabilizes soil surfaces. These interannual patterns highlight the utility of RNDSI for identifying seasonal soiling risks and optimizing cleaning schedules to sustain PV performance in dust-prone environments.

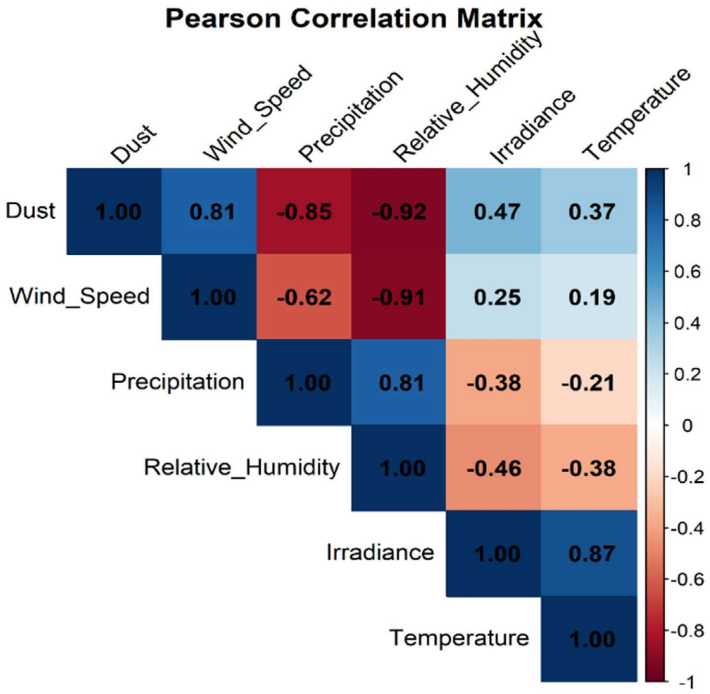

Figure 4. Pearson correlation matrix showing the relationships between dust levels and meteorological parameters (wind speed, precipitation, relative humidity, irradiance, and temperature) in this study area.

5.4. Dust Maps Using Dry Bare Soil Index (from 2021 to 2023)

The DBSI maps for 2021, 2022, and 2023 (Figures 6(a)-(c)) highlight the spatial and temporal variability of dry bare soil exposure across the study area and its relevance to PV soiling. DBSI values are classified into three categories: low (2021: 0.10 - 0.12; 2022: 0.10 - 0.11; 2023: 0.08 - 0.10, green), moderate (0.11 - 0.24, yellow), and high (2021: 0.24 - 0.34; 2022: 0.24 - 0.34; 2023: 0.24 - 0.35, red).

In 2021 (Figure 6(a)), elevated values were most prominent in April, May, and November, reflecting dry, windy conditions and sparse vegetation that favored

dust mobilization, while January, February, and December were dominated by low values, suggesting higher soil moisture and stabilized surfaces. The 2022 (Figure 6(b)) maps revealed peaks in June, October, November, and December, linked to dry soils, reduced vegetation cover, and stronger winds, whereas the January-May period remained relatively stable with predominantly low values. In 2023 (Figure 6(c)), high DBSI levels appeared in March, April, and December, particularly concentrated in the northeast and southeast, while July-September showed widespread low values due to rainfall and vegetation growth. Transitional months such as May and October generally exhibited moderate conditions.

Across all three years, persistent hotspots were associated with exposed soils, unpaved roads, or anthropogenic disturbances, while vegetated or stabilized surfaces consistently aligned with low DBSI values. These patterns emphasize seasonal and interannual variability in dust exposure and highlight the importance of DBSI as a tool for identifying high-risk periods and locations of soiling. Such insights are valuable for aligning PV cleaning and maintenance schedules with dust activity, ensuring more efficient plant operation and optimized resource use in dust-prone environments.

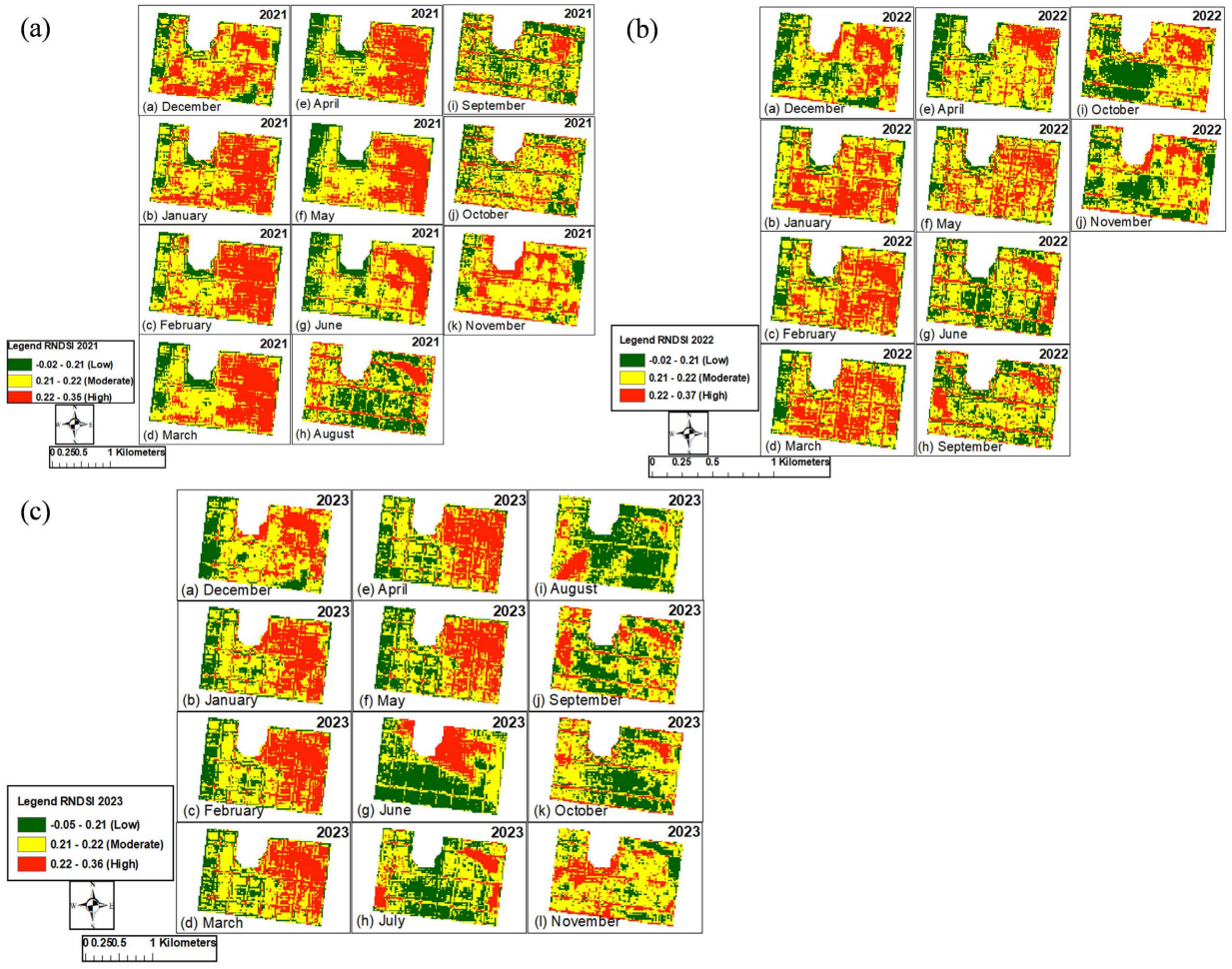

Figure 5. Monthly RNSI maps (2021-2023) showing seasonal dust dynamics and potential PV soiling risk in the Kita solar plant.

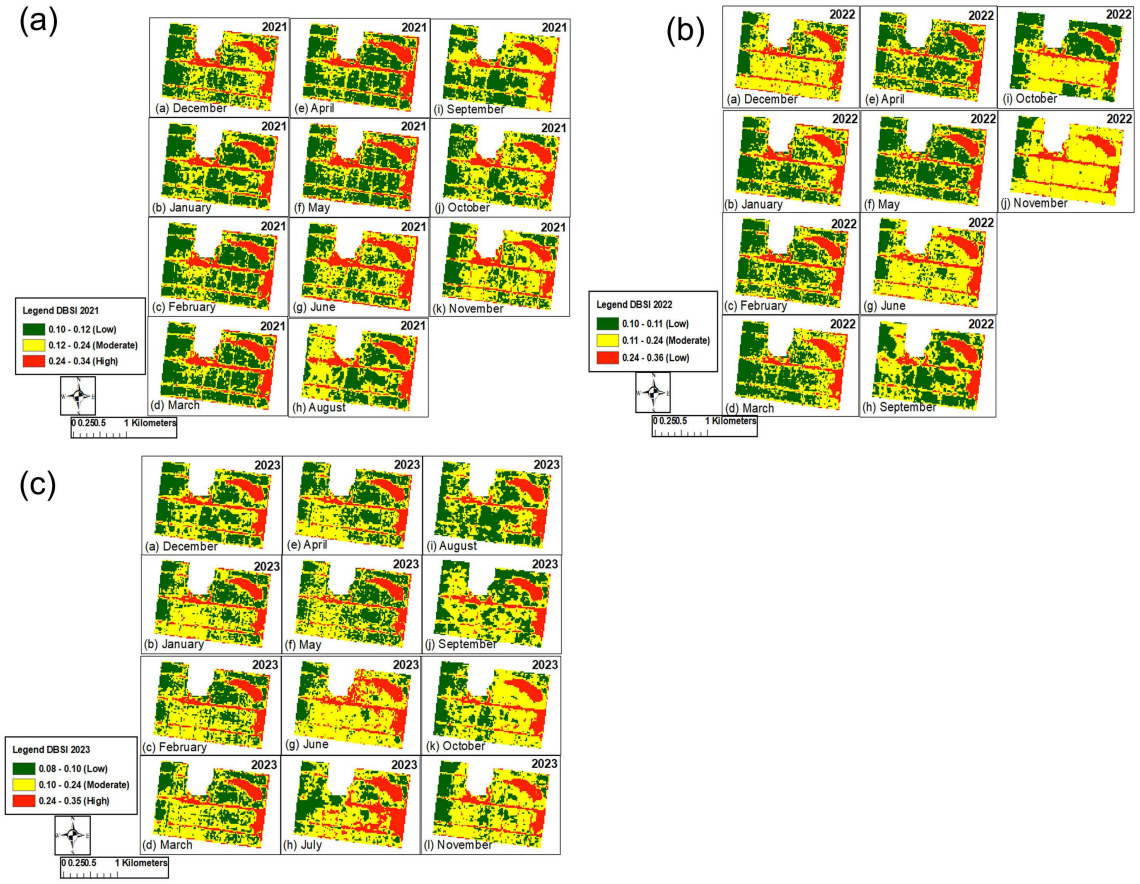

Figure 6. Monthly DBSI maps (2021-2023) showing seasonal dust dynamics and potential PV soiling risk in the Kita solar plant.

6. Discussions

Dust plays a decisive role in regulating solar irradiance and PV performance in West Africa. During the dust storm season (October-January), dense layers significantly reduce surface irradiance, lowering panel efficiency and producing localized cooling, whereas summer months are marked by clearer skies and higher radiation. These dynamics underscore the importance of accounting for dust in solar resource models [43] [44]. Temperature also contributes indirectly: hot months (March-May) enhance convection and uplift, but studies confirm that wind and humidity exert stronger direct control over dust activity [45].

Wind speed emerges as the dominant mobilization factor. Moderate winds, especially the Harmattan (October-May), raise dust concentrations, while extreme winds disperse particles more widely [46] [47]. Rainfall serves as the most effective removal mechanism through wet deposition, supported by vegetation growth during the rainy season [48]. Relative humidity exerts similar suppression, with high moisture promoting aggregation and deposition, and low values sustaining long range transport [48].

Correlation analysis reinforces these dynamics: wind speed strongly enhances dust $(r = 0.81)$, precipitation $(r = -0.85)$ and humidity $(r = -0.92)$ [49] sup-

press it, irradiance shows a moderate positive link $(r = 0.47)$, and temperature contributes weakly but indirectly $(r = 0.37)$ [50] [51]. Interconnections are evident, e.g., strong winds coincide with dry air $(r = -0.91)$, rainfall with higher humidity $(r = 0.81)$, and irradiance with warmer conditions $(r = 0.87)$.

Satellite based indices capture these spatiotemporal patterns. RNDSI peaks (0.22 - 0.35) in December-March and October-November reflect maximum dust deposition and efficiency losses of up to 40% [52] [53]. DBSI highlights bare soil driven risks (0.24 - 0.36) during June and October-December, with persistent hotspots linked to land use [54]. Seasonal and spatial variability observed by both indices (**Figure 5**, **Figure 6**) provide actionable insights for PV maintenance: intensified cleaning during dusty months, reduced intervention in the wet season, and targeted mitigation in exposed zones [55] [56]. RNDSI generally responds more slowly to rainfall events, while DBSI is more sensitive to soil exposure [50] [54].

Finally, limitations must be acknowledged. Sentinel-2's 10 - 20 m resolution can induce mixed-pixel errors in narrow PV arrays [57], and challenges in spatial scaling have been widely documented [58] [59]. Cloud cover during the rainy season may also affect retrieval accuracy [60]. Moreover, the absence of ground based validation data (inverter logs, soiling ratios) due to access restrictions introduces uncertainty. Future research should integrate operator supplied datasets to strengthen validation and improve the robustness of RNDSI/DBSI applications.

7. Conclusions

Saharan dust in Kita (Mali) is deeply influenced by the delicate balance of environmental factors. Wind is the key force driving dust movement, particularly during the dry season, while rainfall plays a cleansing role, clearing the air and resetting the cycle. Humidity, temperature, and sunlight also play supporting roles, shaping the seasonal rhythm of dust activity.

This cycle doesn't just affect the environment, and it has real-world impacts on everything from air quality and nutrient transport to global weather patterns. Dust also presents challenges for solar energy production, as it builds up on solar panels and reduces efficiency. Remote sensing tools like DBSI and RNDSI make it easier to track dust buildup on solar panels and provide valuable insights for planning maintenance. The best time for cleaning is during the peak dust season, from December to May, while the rainy season, from June to September, requires less cleaning as the rain naturally helps to clear the dust.

Recognizing and adapting to these patterns is crucial. From improving climate models to better-managing resources, understanding Saharan dust dynamics helps communities in Kita and beyond respond to its challenges and opportunities. Ongoing research and validation will only strengthen our ability to adapt, making the most of these insights for a healthier and more sustainable future.

Acknowledgements

The authors wish to acknowledge the scholarship and financial support provided

to the First author by the West African Science Service Center on Climate Change and Adapted Land Use (WASCAL) through its graduate research programme on Energy at UAM, Niamey. Authors are grateful for the kind cooperation of all the institutions and agencies providers of data.

Conflicts of Interest

The authors declare no conflicts of interest.

References

[1] Supe, H., Avtar, R., Singh, D., Gupta, A., Yunus, A.P., Dou, J., *et al.* (2020) Google Earth Engine for the Detection of Soiling on Photovoltaic Solar Panels in Arid Environments. *Remote Sensing*, **12**, Article 1466. https://doi.org/10.3390/rs12091466

[2] Adekanbi, M.L., Alaba, E.S., John, T.J., Tundealao, T.D. and Banji, T.I. (2024) Soiling Loss in Solar Systems: A Review of Its Effect on Solar Energy Efficiency and Mitigation Techniques. *Cleaner Energy Systems*, **7**, Article 100094. https://doi.org/10.1016/j.cles.2023.100094

[3] Abuzaid, H., Awad, M. and Shamayleh, A. (2024) Photovoltaic Modules' Cleaning Method Selection for the MENA Region. *Sustainability*, **16**, 9331. https://doi.org/10.3390/su16219331

[4] Saidan, M., Albaali, A.G., Alasis, E. and Kaldellis, J.K. (2016) Experimental Study on the Effect of Dust Deposition on Solar Photovoltaic Panels in Desert Environment. *Renewable Energy*, **92**, 499-505. https://doi.org/10.1016/j.renene.2016.02.031

[5] Dantas, G.M., Mendes, O.L.C., Maia, S.M. and De Alexandria, A.R. (2020) Dust Detection in Solar Panel Using Image Processing Techniques: A Review. *Research, Society and Development*, **9**, e321985107. https://doi.org/10.33448/rsd-v9i8.5107

[6] Shah, M., Joshi, M., Patel, P., Mevada, N., Baria, R. and Chauhan, M. (2023) Improving Solar Power Generation with Inceptionv3 Dust Detection on the Solar Panel Energy Systems. 2023 *Third International Conference on Ubiquitous Computing and Intelligent Information Systems* (*ICUIS*), Gobichettipalayam, 1-2 September 2023, 448-456. https://doi.org/10.1109/icuis60567.2023.00080

[7] Abuqaaud, K.A. and Ferrah, A. (2020) A Novel Technique for Detecting and Monitoring Dust and Soil on Solar Photovoltaic Panel. 2020 *Advances in Science and Engineering Technology International Conferences* (*ASET*), Dubai, 4 February 2020-9 April 2020, 1-6. https://doi.org/10.1109/aset48392.2020.9118377

[8] Liu, X., Cui, L., Tao, Q., Yi, Z., Li, J. and Lu, L. (2023) Dust Deposition Mechanism and Output Characteristics of Solar Bifacial PV Panels. *Environmental Science and Pollution Research*, **30**, 100937-100949. https://doi.org/10.1007/s11356-023-29518-1

[9] Fadhil, A.M. (2013) Sand Dunes Monitoring Using Remote Sensing and GIS Techniques for Some Sites in Iraq. *Third International Conference on Photonics and Image in Agriculture Engineering*, Sanya, 19 March 2013, 876206.

[10] Wu, S., Chen, H. and Peng, K. (2023) Effect of Dust Deposition on Solar Panel in Solar Power Generation. *Sensors and Materials*, **35**, Article 2371. https://doi.org/10.18494/sam4441

[11] Shairi, N.A.S., Ghoni, R. and Ali, K. (2020) Solar Panel Dust Monitoring System. *Engineering Heritage Journal*, **4**, 44-45. https://doi.org/10.26480/gwk.02.2020.44.45

[12] Luo, W., Khoo, Y. S., Hacke, P., Naumann, V., Lausch, D., Harvey, S. P., *et al.* (2017) Potential-Induced Degradation in Photovoltaic Modules: A Critical Review. *Energy*

& Environmental Science, **10**, 43-68. https://doi.org/10.1039/C6EE02271E

[13] Ellabban, O., Abu-Rub, H. and Blaabjerg, F. (2014) Renewable Energy Resources: Current Status, Future Prospects and Their Enabling Technology. *Renewable and Sustainable Energy Reviews*, **39**, 748-764. https://doi.org/10.1016/j.rser.2014.07.113

[14] Al Garni, H.Z. (2022) The Impact of Soiling on PV Module Performance in Saudi Arabia. *Energies*, **15**, Article 8033. https://doi.org/10.3390/en15218033

[15] Kazem, H.A., Chaichan, M.T., Al-Waeli, A.H.A. and Sopian, K. (2020) A Review of Dust Accumulation and Cleaning Methods for Solar Photovoltaic Systems. *Journal of Cleaner Production*, **276**, Article 123187. https://doi.org/10.1016/j.jclepro.2020.123187

[16] Benghanem, M., Almohammedi, A., Taukeer Khan, M. and Al-Masraqi, A. (2018) Effect of Dust Accumulation on the Performance of Photovoltaic Panels in Desert Countries: A Case Study for Madinah, Saudi Arabia. *International Journal of Power Electronics and Drive Systems* (*IJPEDS*), **9**, Article 1356. https://doi.org/10.11591/ijpeds.v9.i3.pp1356-1366

[17] Souza, T.L.S.d., Lima, R.L.F.A. and Lima Júnior, C.d. (2022) Dirt on Photovoltaic Modules and Efficient Energy Generation in the Brazilian Semiarid. *Revista Brasileira de Engenharia Agrícola e Ambiental*, **26**, 321-326. https://doi.org/10.1590/1807-1929/agriambi.v26n5p321-326

[18] Vedulla, G., Geetha, A. and Senthil, R. (2022) Review of Strategies to Mitigate Dust Deposition on Solar Photovoltaic Systems. *Energies*, **16**, Article 109. https://doi.org/10.3390/en16010109

[19] Kazem, H.A., Chaichan, M.T., Al-Waeli, A.H.A., Al-Badi, R., Fayad, M.A. and Gholami, A. (2022) Dust Impact on Photovoltaic/thermal System in Harsh Weather Conditions. *Solar Energy*, **245**, 308-321. https://doi.org/10.1016/j.solener.2022.09.012

[20] Ali, H., Zafar, M., Bashir, M., Nasir, M., Ali, M. and Siddiqui, A. (2017) Effect of Dust Deposition on the Performance of Photovoltaic Modules in Taxila, Pakistan. *Thermal Science*, **21**, 915-923. https://doi.org/10.2298/tsci140515046a

[21] Kruitwagen, L., Story, K.T., Friedrich, J., Byers, L., Skillman, S. and Hepburn, C. (2021) A Global Inventory of Photovoltaic Solar Energy Generating Units. *Nature*, **598**, 604-610. https://doi.org/10.1038/s41586-021-03957-7

[22] Seutloali, K.E., Dube, T. and Sibanda, M. (2018) Developments in the Remote Sensing of Soil Erosion in the Perspective of Sub-Saharan Africa. Implications on Future Food Security and Biodiversity. *Remote Sensing Applications*: *Society and Environment*, **9**, 100-106. https://doi.org/10.1016/j.rsase.2017.12.002

[23] Symeonakis, E. and Drake, N. (2004) Monitoring Desertification and Land Degradation over Sub-Saharan Africa. *International Journal of Remote Sensing*, **25**, 573-592. https://doi.org/10.1080/0143116031000095998

[24] Gómez, D., Salvador, P., Sanz, J., Casanova, C. and Casanova, J.L. (2018) Detecting Areas Vulnerable to Sand Encroachment Using Remote Sensing and GIS Techniques in Nouakchott, Mauritania. *Remote Sensing*, **10**, Article 1541. https://doi.org/10.3390/rs10101541

[25] Dewitte, O., Jones, A., Elbelrhiti, H., Horion, S. and Montanarella, L. (2012) Satellite Remote Sensing for Soil Mapping in Africa. *Progress in Physical Geography*: *Earth and Environment*, **36**, 514-538. https://doi.org/10.1177/0309133312446981

[26] Khechba, K., Laamrani, A., Dhiba, D., Misbah, K. and Chehbouni, A. (2021) Monitoring and Analyzing Yield Gap in Africa through Soil Attribute Best Management

Using Remote Sensing Approaches: A Review. *Remote Sensing*, **13**, Article 4602. https://doi.org/10.3390/rs13224602

[27] Edwards, M.R., Holloway, T., Pierce, R.B., Blank, L., Broddle, M., Choi, E., *et al.* (2022) Satellite Data Applications for Sustainable Energy Transitions. *Frontiers in Sustainability*, **3**, Article ID: 910924. https://doi.org/10.3389/frsus.2022.910924

[28] Zinzendoff Okwonu, F., Laro Asaju, B. and Irimisose Arunaye, F. (2020) Breakdown Analysis of Pearson Correlation Coefficient and Robust Correlation Methods. *IOP Conference Series*: *Materials Science and Engineering*, **917**, Article 012065. https://doi.org/10.1088/1757-899x/917/1/012065

[29] Rasul, A., Balzter, H., Ibrahim, G.R.F., Hameed, H.M., Wheeler, J., Adamu, B., *et al.* (2018) Applying Built-Up and Bare-Soil Indices from Landsat 8 to Cities in Dry Climates. *Land*, **7**, Article 81. https://doi.org/10.3390/land7030081

[30] Deng, Y., Wu, C., Li, M. and Chen, R. (2015) RNDSI: A Ratio Normalized Difference Soil Index for Remote Sensing of Urban/Suburban Environments. *International Journal of Applied Earth Observation and Geoinformation*, **39**, 40-48. https://doi.org/10.1016/j.jag.2015.02.010

[31] Mejia, F., Kleissl, J. and Bosch, J.L. (2014) The Effect of Dust on Solar Photovoltaic Systems. *Energy Procedia*, **49**, 2370-2376. https://doi.org/10.1016/j.egypro.2014.03.251

[32] Csavina, J., Field, J., Félix, O., Corral-Avitia, A.Y., Sáez, A.E. and Betterton, E.A. (2014) Effect of Wind Speed and Relative Humidity on Atmospheric Dust Concentrations in Semi-Arid Climates. *Science of The Total Environment*, **487**, 82-90. https://doi.org/10.1016/j.scitotenv.2014.03.138

[33] Yang, X., Zhou, C., Huo, W., Yang, F., Liu, X. and Mamtimin, A. (2019) A Study on the Effects of Soil Moisture, Air Humidity, and Air Temperature on Wind Speed Threshold for Dust Emissions in the Taklimakan Desert. *Natural Hazards*, **97**, 1069-1081. https://doi.org/10.1007/s11069-019-03686-1

[34] Opp, C., Groll, M., Abbasi, H. and Foroushani, M.A. (2021) Causes and Effects of Sand and Dust Storms: What Has Past Research Taught Us? a Survey. *Journal of Risk and Financial Management*, **14**, Article 326. https://doi.org/10.3390/jrfm14070326

[35] Wang, Y., Xia, W. and Zhang, G.J. (2021) What Rainfall Rates Are Most Important to Wet Removal of Different Aerosol Types? *Atmospheric Chemistry and Physics*, **21**, 16797-16816. https://doi.org/10.5194/acp-21-16797-2021

[36] Ma, X., Gao, Q., Jiang, X., Chen, S., Gan, Y., Zhang, T., *et al.* (2023) Direct Effects of Air Humidity on Dust Aerosol Production: Evidences for the Surprising Role of Electrostatic Forces. *Geophysical Research Letters*, **50**, e2023GL103639. https://doi.org/10.1029/2023gl103639

[37] Shao, Y. (2024) Adhesion Theory and Model for Air Humidity Impact on Dust Emission. *Aeolian Research*, **66**, Article 100898. https://doi.org/10.1016/j.aeolia.2024.100898

[38] Li, H. and Wang, C. (2022) Impact of Dust Radiation Effect on Simulations of Temperature and Wind—A Case Study in Taklimakan Desert. *Atmospheric Research*, **273**, Article 106163. https://doi.org/10.1016/j.atmosres.2022.106163

[39] Kok, J.F., Ward, D.S., Mahowald, N.M. and Evan, A.T. (2018) Global and Regional Importance of the Direct Dust-Climate Feedback. *Nature Communications*, **9**, Article No. 241. https://doi.org/10.1038/s41467-017-02620-y

[40] Gkikas, A., Obiso, V., Pérez García-Pando, C., Jorba, O., Hatzianastassiou, N., Vendrell, L., *et al.* (2018) Direct Radiative Effects during Intense Mediterranean De-

sert Dust Outbreaks. *Atmospheric Chemistry and Physics*, **18**, 8757-8787. https://doi.org/10.5194/acp-18-8757-2018

[41] Yang, Y., Ni, C., Jiang, M. and Chen, Q. (2021) Effects of Aerosols on the Atmospheric Boundary Layer Temperature Inversion over the Sichuan Basin, China. *Atmospheric Environment*, **262**, Article 118647. https://doi.org/10.1016/j.atmosenv.2021.118647

[42] Friese, C.A., van der Does, M., Merkel, U., Iversen, M.H., Fischer, G. and Stuut, J.W. (2016) Environmental Factors Controlling the Seasonal Variability in Particle Size Distribution of Modern Saharan Dust Deposited off Cape Blanc. *Aeolian Research*, **22**, 165-179. https://doi.org/10.1016/j.aeolia.2016.04.005

[43] Mbourou, G.N., Bertrand, J.J. and Nicholson, S.E. (1997) The Diurnal and Seasonal Cycles of Wind-Borne Dust over Africa North of the Equator. *Journal of Applied Meteorology*, **36**, 868-882. https://doi.org/10.1175/1520-0450(1997)036<0868:tdasco>2.0.co;2

[44] Clauzel, L., Anquetin, S., Lavaysse, C., *et al.* (2025) Solar Radiation Estimation in West Africa: Impact of Dust Conditions during 2021 Dry Season. *Atmospheric Chemistry and Physics*, **25**, 997-1021. https://doi.org/10.5194/acp-25-997-2025

[45] Neher, I., Crewell, S., Meilinger, S., Pfeifroth, U. and Trentmann, J. (2020) Photovoltaic Power Potential in West Africa Using Long-Term Satellite Data. *Atmospheric Chemistry and Physics*, **20**, 12871-12888. https://doi.org/10.5194/acp-20-12871-2020

[46] Schwanghart, W. and Schütt, B. (2008) Meteorological Causes of Harmattan Dust in West Africa. *Geomorphology*, **95**, 412-428. https://doi.org/10.1016/j.geomorph.2007.07.002

[47] Oluleye, A. and Folorunsho, A. (2019) Influence of Atmospheric Dynamic Factors on Dust Aerosol Mobilization over West Africa: Simulations from WRF-Chem. *Aerosol Science and Engineering*, **3**, 132-149. https://doi.org/10.1007/s41810-019-00048-z

[48] Marticorena, B., Chatenet, B., Rajot, J.L., Traoré, S., Coulibaly, M., Diallo, A., *et al.* (2010) Temporal Variability of Mineral Dust Concentrations over West Africa: Analyses of a Pluriannual Monitoring from the AMMA Sahelian Dust Transect. *Atmospheric Chemistry and Physics*, **10**, 8899-8915. https://doi.org/10.5194/acp-10-8899-2010

[49] Middleton, N.J. and Goudie, A.S. (2001) Saharan Dust: Sources and Trajectories. *Transactions of the Institute of British Geographers*, **26**, 165-181. https://doi.org/10.1111/1475-5661.00013

[50] Marticorena, B., Chatenet, B., Rajot, J.L., Bergametti, G., Deroubaix, A., Vincent, J., *et al.* (2017) Mineral Dust over West and Central Sahel: Seasonal Patterns of Dry and Wet Deposition Fluxes from a Pluriannual Sampling (2006-2012). *Journal of Geophysical Research: Atmospheres*, **122**, 1338-1364. https://doi.org/10.1002/2016jd025995

[51] Muñoz-García, M., Fouris, T. and Pilat, E. (2021) Analysis of the Soiling Effect under Different Conditions on Different Photovoltaic Glasses and Cells Using an Indoor Soiling Chamber. *Renewable Energy*, **163**, 1560-1568. https://doi.org/10.1016/j.renene.2020.10.027

[52] Jickells, T.D., An, Z.S., Andersen, K.K., Baker, A.R., Bergametti, G., Brooks, N., *et al.* (2005) Global Iron Connections between Desert Dust, Ocean Biogeochemistry, and Climate. *Science*, **308**, 67-71. https://doi.org/10.1126/science.1105959

[53] Schepanski, K., Tegen, I., Todd, M.C., Heinold, B., Bönisch, G., Laurent, B., *et al.* (2009) Meteorological Processes Forcing Saharan Dust Emission Inferred from MSG-

SEVIRI Observations of Subdaily Dust Source Activation and Numerical Models. *Journal of Geophysical Research*: *Atmospheres*, **114**, 2008JD010325. https://doi.org/10.1029/2008jd010325

[54] Prospero, J.M. and Lamb, P.J. (2003) African Droughts and Dust Transport to the Caribbean: Climate Change Implications. *Science*, **302**, 1024-1027. https://doi.org/10.1126/science.1089915

[55] Elminir, H.K., Ghitas, A.E., Hamid, R.H., El-Hussainy, F., Beheary, M.M. and Abdel-Moneim, K.M. (2006) Effect of Dust on the Transparent Cover of Solar Collectors. *Energy Conversion and Management*, **47**, 3192-3203. https://doi.org/10.1016/j.enconman.2006.02.014

[56] Kaldellis, J.K. and Kapsali, M. (2011) Simulating the Dust Effect on the Energy Performance of Photovoltaic Generators Based on Experimental Measurements. *Energy*, **36**, 5154-5161. https://doi.org/10.1016/j.energy.2011.06.018

[57] Jiang, H., Yao, L., Lu, N., Qin, J., Liu, T., Liu, Y., *et al.* (2021) Multi-Resolution Dataset for Photovoltaic Panel Segmentation from Satellite and Aerial Imagery. *Earth System Science Data*, **13**, 5389-5401. https://doi.org/10.5194/essd-13-5389-2021

[58] Tarasiewicz, T., Nalepa, J., Farrugia, R.A., Valentino, G., Chen, M., Briffa, J.A., *et al.* (2023) Multitemporal and Multispectral Data Fusion for Super-Resolution of Sentinel-2 Images. *IEEE Transactions on Geoscience and Remote Sensing*, **61**, 1-19. https://doi.org/10.1109/tgrs.2023.3311622

[59] Chanev, M., Kamenova, I., Dimitrov, P. and Filchev, L. (2025) Evaluation of Sentinel-2 Deep Resolution 3.0 Data for Winter Crop Identification and Organic Barley Yield Prediction. *Remote Sensing*, **17**, Article 957. https://doi.org/10.3390/rs17060957

[60] Zhu, Z. and Woodcock, C.E. (2012) Object-Based Cloud and Cloud Shadow Detection in Landsat Imagery. *Remote Sensing of Environment*, **118**, 83-94. https://doi.org/10.1016/j.rse.2011.10.028